Journal of the European Ceramic Society 42 (2022) 3015–3022

Contents lists available at ScienceDirect

Journal of the European Ceramic Society

journal homepage: www.elsevier.com/locate/jeurceramsoc

Jun ware glaze colours: An X-ray absorption spectroscopy study

Mingyue Yuan [a], Jiayu Hou [b], Giulio Gorni [c], Daniel Crespo [a], Yuan Li [b], Trinitat Pradell [a,*]

[a] Physics Department and Barcelona Research Centre in Multiscale Science and Engineering, Universitat Politècnica de Catalunya BarcelonaTech, Campus Diagonal-Besòs, c) Eduard Maristany 16, 08930 Barcelona, Spain
[b] The Palace Museum and Key Scientific Research Base of Ancient Ceramics, State Administration of Cultural Heritage, Beijing, China
[c] CELLS-ALBA Synchrotron, Carrer de la Llum 2–26, 08290 Barcelona, Cerdanyola del Vallès, Spain

ARTICLE INFO

Keywords:
Fe K-pre-edge fitting
Metallic copper nanoparticles
Iron oxidation state
Absorption and scattering
Glass nanostructure, Jun ware glaze

ABSTRACT

Jun ware is stoneware created in the late Northern Song dynasty (12th century) with a blue glaze combining transparent-blue and whitish-opaque submillimetric areas.

The glaze has a glass nanostructure with lime-rich droplets in a silica-rich matrix resulting from a high temperature liquid-liquid phase separation. Calcium-rich opaque and calcium-poor transparent areas are combined. Iron is more oxidised in the calcium rich areas (≈17–20% Fe^{2+}) than in the calcium poor areas (≈60–70% Fe^{2+}) of the glaze. Therefore, iron is oxidised in the lime-rich droplets and reduced in the silica-rich matrix. The *sky*-like appearance of the glaze is due to the combination of the light absorption in the transparent-dark-blue Fe^{2+} rich areas and scattering in the white-yellowish Fe^{3+} rich areas.

Copper appears mainly oxidised but in the red areas a few small copper nanoparticles are present and iron appears more oxidised. The result indicates the simultaneous reduction of copper and oxidation of iron.

1. Introduction

Jun ware is one of the five famous wares created in the Northern Song dynasty (960–1127) in the first quarter of the 12th century [1–3], and which continued being produced during the Jin (1115–1234), Yuan (1271–1368) and early Ming (1368–1435) Dynasties. Jun ware is a high-fired grey-bodied stoneware with a subtle high temperature glaze of a pale bluish tone [1–3]. Finally, red and purple colours were obtained adding copper to the glazes, either as brush strokes or as a layer applied on the surface (Fig. 1).

The blue glaze combining transparent-blue and whitish-opaque submillimetric areas (some tens of micrometres) give to the glaze a *sky*-like appearance (Fig. 1). Opacity results from scattering of the glass nanostructure [4] developed due to the high SiO_2:Al_2O_3 ratio (above 7:1), which, when fired at temperatures of about 1200 °C, undergoes a liquid-liquid phase separation [4–8]. Two glass nanostructures, a lime rich (enriched also in Fe, Mg, P and Ti) and a silica rich (enriched also in K and Na) were reported [4,9] (Fig. 1), similarly to what is found in basaltic systems [4,10–12]. A recent study of the nanostructure of Jun glazes [4] has shown that a higher CaO content is responsible for a greater volume fraction of lime rich larger droplets (isolated or interconnected) and the different refraction indices of the two glasses for the scattering of the light, the so-called Mie scattering. The light travels thorough the glaze until it is scattered in the nanostructure (after multiple scattering processes) or absorbed by the metal ions present in the glaze. The back-scattered light eventually reaches the surface of the glaze and, consequently, a large volume fraction of droplets produces a high total diffuse reflectance (more lightness and opacity) [4].

As different submillimetric (tens of micrometres) areas of the glaze contained various amounts of CaO, more and larger droplets form in the calcium rich areas (more opaque) while smaller and fewer droplets are present in the calcium poorer areas (more transparent). Consequently, the final colour (dark or light blue) and the pearly translucency to the glazes results from the combination of submillimetric calcium rich and poor areas and the blue colour given by Fe^{2+} ions dissolved in the glaze is responsible for the blue colour (large and broad Fe^{2+} absorption NIR band at 1100 nm extending in the red) [13,14]. Assuming that iron is mainly present in its reduced state.

Another characteristic of Jun ware glaze is that the reaction between the glaze and the stoneware ceramic gives rise to chemical interdiffusion, so that an Al_2O_3 richer (SiO_2:Al_2O_3 < 7) dark olive-brown glaze layer is formed at the interface which does not show glass nanostructure (Fig. 1) [3,4,7–9]. The brown colour is due to the incorporation of TiO_2 from the ceramic and the simultaneous oxidation of Fe^{2+}

* Corresponding author.
E-mail address: Trinitat.Pradell@upc.edu (T. Pradell).

https://doi.org/10.1016/j.jeurceramsoc.2022.02.016
Received 13 December 2021; Received in revised form 29 January 2022; Accepted 4 February 2022
Available online 8 February 2022

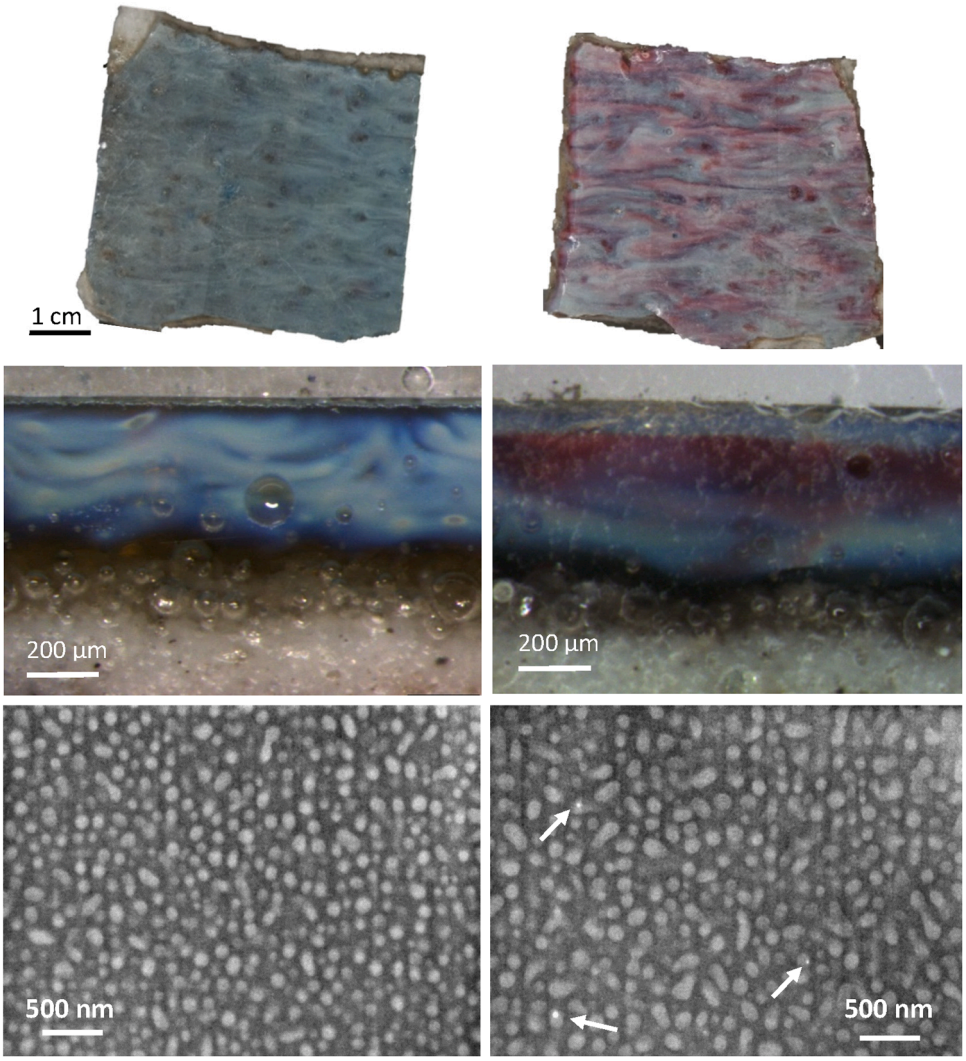

Fig. 1. (Top) Surface appearance of the blue and red side from JS24. (Middle) Cross section and (Bottom) nanostructure of the blue (left) and red (right) glazes. The white droplets are calcium rich in a darker silica rich matrix. Small precipitates of metal copper nanoparticles are present in the red glaze. (For interpretation of the references to colour in this figure legend, the reader is referred to the web version of this article.)

into Fe^{3+} and reduction of Ti^{4+} into Ti^{3+} [15,16]. Mössbauer spectroscopic analysis of the blue and some brown-greenish Jun glazes proved that the brown glaze is more oxidised than the blue glaze [4]. However, Mössbauer spectroscopy is a macroscopic analytical technique and, therefore, the Fe oxidation state in the submillimetric calcium rich and poor areas of the glazes could not be obtained.

In fact, it has recently been highlighted that the amount of titanium content of Jun ware glazes (>0.2% TiO_2) is high enough to switch the colour of Jun ware glazes (≈2.0% FeO) from blue to green like happens in other celadons (lime glazes) [17]. The answer to this anomaly has recently been related to the concentration of titanium in the lime-rich. However, being the oxidation state of iron in the calcium rich and poor areas of the glaze unknown, the explanation is not satisfactory.

Finally, the red and purple colours have mainly been associated with the presence of cuprite [7] or of copper metal nanoparticles. In fact, recently, the presence of copper metal nanoparticles in the red and purple glazes was verified [4] (Fig. 1). Copper nanoparticles are characterized by Surface Plasmon Resonance (SPR) extinction peak at 560 nm [18] which absorbs the yellow light giving a red tinge to the glaze. Iron and copper ions may be present in the glazes as Cu^{2+}, Cu^{+}, Cu^{o}, Fe^{2+} and Fe^{3+} and react among them. The species present in the different coloured areas of the glazes have not yet been studied.

The striking appearance of Jun glazes is related to their peculiar optical properties and therefore to the scattering of light in the nanostructure but also to the light absorbed by the metal ions present. The role of the nanostructure in the optical properties has been the object of a previous study [4], but the oxidation state of iron in the glazes is not yet fully understood. In fact, although some glazes were analysed by Mössbauer spectroscopy, the oxidation state of iron in the lime-rich and silica-rich nanostructures could not be obtained. Consequently, their role in the colour and appearance of the glazes is still unknown.

The paper is devoted to explore the oxidation state of iron and of copper in Jun ware glazes at a microscopic level and the precipitation of metallic copper nanoparticles and their role in the colour and appearance of the glazes. An X-ray spectroscopic (XAS) study of both iron and copper is performed. The data obtained will be complemented by chemical analyses of the glazes and spectroscopic study in the ultraviolet and visible range.

2. Experimental methodology

A selection of Jun ware samples belonging to the collection of the Palace Museum in Beijing. They were excavated at Yuzhou (Henan). Five shards from the excavation of the Juntai kiln (JS24, JS26, JS27, JS77 and JS78) [19] and one sample (JS4) from the excavation of the Liujiamen kiln. The blue glazes from JS24 (Fig. 1), JS26, JS27, JS77 and

JS4, the brown glaze from JS78 and the red glaze from JS24 were analysed.

XAS spectra at Fe K-edge were collected at the CLAESS beamline (Alba-CELLS synchrotron) [20]. The energy was selected with a Si (111) monochromator with energy resolution better than the width of the corresponding Kα lines. Harmonic rejection was obtained by choosing proper angle and coating of a vertical collimating and vertical focusing mirror. The spot size was adjusted to be around 500 (H) x 300 (V) μm^2. Fe K-edge absorption spectra were collected in fluorescence mode (45ºC detection angle) from the glazes and the fluorescent signal collected by a silicon drift detector (SDD). Additionally, Fe K-edge absorption spectra from several iron standards (Fe foil, Fe_2O_3, FeOOH, Fe_3O_4, and FeO) were collected in transmission mode using two ionization chambers to detect the incident and transmitted intensity. All spectra were calibrated to the first inflection point in a simultaneously measured Fe foil. Data analysis was performed using the Athena and Artemis software [21].

Additionally, using a smaller beam size,200(H) x 100(V) μm^2, sub-millimetric glaze features were also measured. In order to select the areas, X-ray Fluorescence maps from the JS24 blue and red glazes were previously recorded. Then, both Fe K-edge and Cu K-edge absorption spectra were obtained from the selected areas. The energy scans at Fe K-edge were performed from 7005 to 7708 eV and at Cu K-edge from 8870 to 9575 eV.

The pre-edge feature of the Fe K-edge absorption is particularly sensitive to the valence state and local geometry. The pre-peak area and the average peak position is known to shift to higher energy as the ratio of ferric to ferrous iron increases; and a variogram where the average peak positions (centroids) are plotted against total integrated area can be drawn [22] giving an estimation of the different species and their coordination state. Furthermore, a quantification of the Fe^{2+}/Fe ratio can be obtained provided that an empirical calibration is available for reference materials of known oxidation state. In glasses, where both Fe^{3+} and Fe^{2+} are present and the coordination geometry is poorly constrained, a glass-based calibration is preferred to crystalline materials [23–26]. Considering that Jun glazes have a double silica-rich/lime-rich glass nanostructure, the use of a similar glass for the calibration is preferable. In our case, some of the blue Jun ware glazes were previously measured by Mössbauer spectroscopy [4] and they will be used to estimate the oxidation state of the other glazes.

The pre-edge region of the normalized X-ray absorption near-edge structure (XANES) spectra was analysed developing a python code based on procedures described in literature [22,23,27]. The absorption edge onset was modelled by fitting the energy regions below and above the pre-edge feature with an inclined arctangent function [27], then the peaks were fitted using a Voigt profile which is the convolution of the Lorentzian peak related to the lifetime broadening of the 1s→3d electronic transition (with typical FWHM≈1 eV) [24] with a Gaussian contribution from the experimental set-up. In our code, an exact Voigt profile has been used instead of the analytical pseudo-Voigt profile. Profile fitting was performed by using the Trust Region Reflective algorithm, as implemented in the scipy.optimize standard python library [28]. The region fitted was selected between 7100 eV and 7118–7124 eV depending on the edge position. Considering the number of variables involved, imposing some restriction to the number of experimental parameters is advisable. For this reason, the Full Width at Half Maximum (FWHM) and Gaussian fraction were constrained to be shared by all peaks. Moreover, the Gaussian contribution dominates the peak profile of the pre-edge spectrum (X_G >0.9) measured in standard resolution [27]. For this reason, we decided to fix the gaussian contribution to 1. Nevertheless, the results obtained did not vary substantially fixing a lower Gaussian contribution or even leaving it as a free parameter of the fit.

The copper speciation was obtained from the analyses of the Cu K-edge XAS spectra. Copper is normally present in the glaze as Cu^+ and Cu^{2+} in fact, a redox equilibrium between them is known to happen depending on the composition of the glass and the presence of other

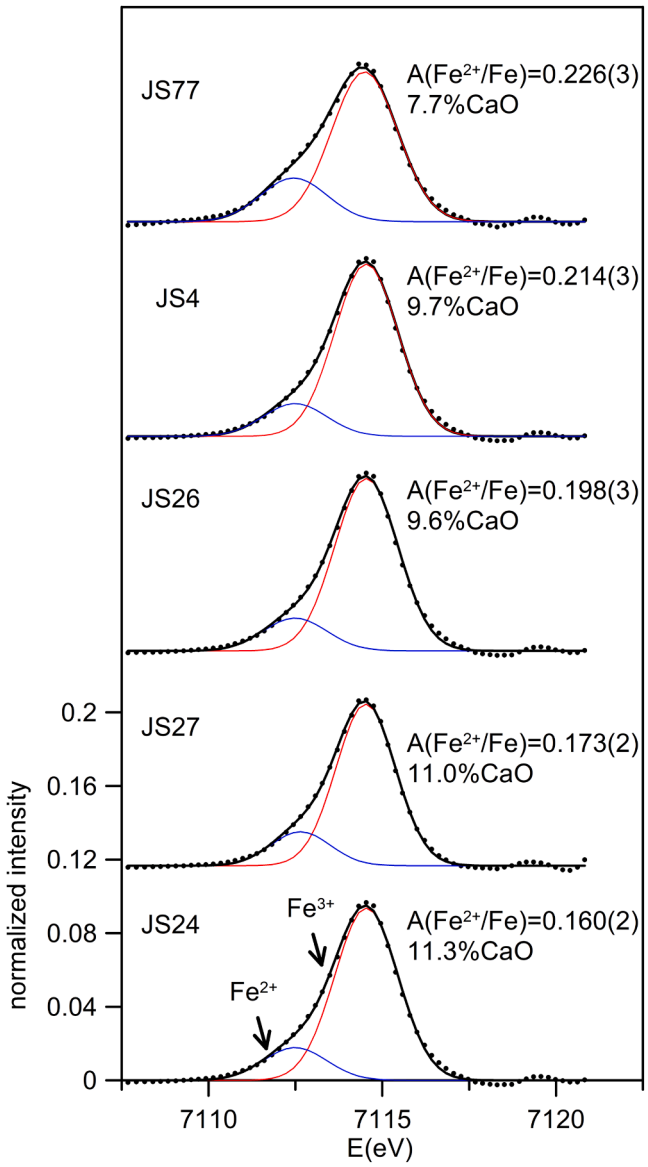

Fig. 2. Fitted pre-edge peaks corresponding to the Jun ware blue glazes.

transition metal ions is expected. The reducing conditions to which the glazes are subjected during the firing result in the precipitation of copper metal nanoparticles, Cu^0. In this case, the EXAFS spectrum has been fitted rather than XANES. Fitting the XANES signal by linear combination of cuprite, tenorite and metal copper does not give a very good result, probably because neither tenorite nor cuprite structures are present in the glass. Moreover, the copper nanoparticles are very small (≈20 nm), consequently, have a large surface/volume ratio which reduce the metal copper contribution to the spectrum.

Nevertheless, the amplitude of the EXAFS oscillations in the spectra was not very high, making it difficult to fit more than the first (Cu-O) shell, and suggesting a lack of any longer-range order which would be consistent with partially reduced oxide dissolved in the glaze. EXAFS fitting was carried out with Artemis software. The spectrum as a linear combination of model compounds each weighted by each compound fraction and the sum set equal to 1 [29].

The chemical composition and nanostructure of the glazes were obtained using a crossbeam workstation (Zeiss Neon 40) equipped with Scanning Electron Microscope (SEM) (Shottky FE) and Gallium Focus Ion Beam (Ga-FIB) columns. Polished areas of the glazes were obtained using the Ga ions, acceleration voltage 30 kV, from which Secondary

Table 1
Fitted pre-edge data corresponding the blue Jun ware glazes. fwhm, E_1, E_2, A_1, A_1 are the full width at half maximum, energy and area of the fitted peaks; C, A and A (Fe^{2+}/Fe) are the centre shift, total area and Fe^{2+} peak area fraction. [1] Fraction of Fe^{2+} calculated from the XANES data[a] using the Mössbauer data[2]. Sample JS4 corresponds to the opposite side of that referred in [4]; this explains the different Fe^{2+}/Fe_{total} ratio[3].

sample	fwhm		Fe^{3+}				Fe^{2+}				C		A		A (Fe^{2+}/Fe)[a]		Fe^{2+}/Fe_{total}[1]		Fe^{2+}/Fe_{total}[2]
	(eV)		E_1 (eV)		A_1 (eV)		E_2 (eV)		A_2 (eV)		(eV)		(eV)				(%)		(%)
JS24	1.82	(3)	7113.62	(1)	0.18	(1)	7111.57	(5)	0.044	(3)	7113.29	(2)	0.255	(4)	0.160	(2)	43	(4)	
JS26	1.61	(2)	7113.62	(1)	0.25	(1)	7111.76	(5)	0.053	(3)	7113.25	(1)	0.243	(4)	0.198	(2)	65	(4)	
JS27	1.71	(2)	7113.60	(1)	0.15	(1)	7111.72	(5)	0.054	(3)	7113.28	(1)	0.228	(3)	0.173	(2)	51	(3)	
JS4	1.80	(2)	7113.60	(1)	0.22	(1)	7111.69	(6)	0.050	(3)	7113.19	(1)	0.245	(4)	0.214	(2)	74	(4)	73(2)[3]
JS77	1.90	(2)	7113.57	(2)	0.26	(1)	7111.53	(6)	0.043	(2)	7113.11	(2)	0.251	(5)	0.226	(3)	81	(5)	82(3)
JS78	1.80	(3)	7113.59	(1)	0.32	(1)	7111.52	(5)	0.063	(3)	7113.33	(2)	0.237	(4)	0.125	(2)	22	(4)	23(3)

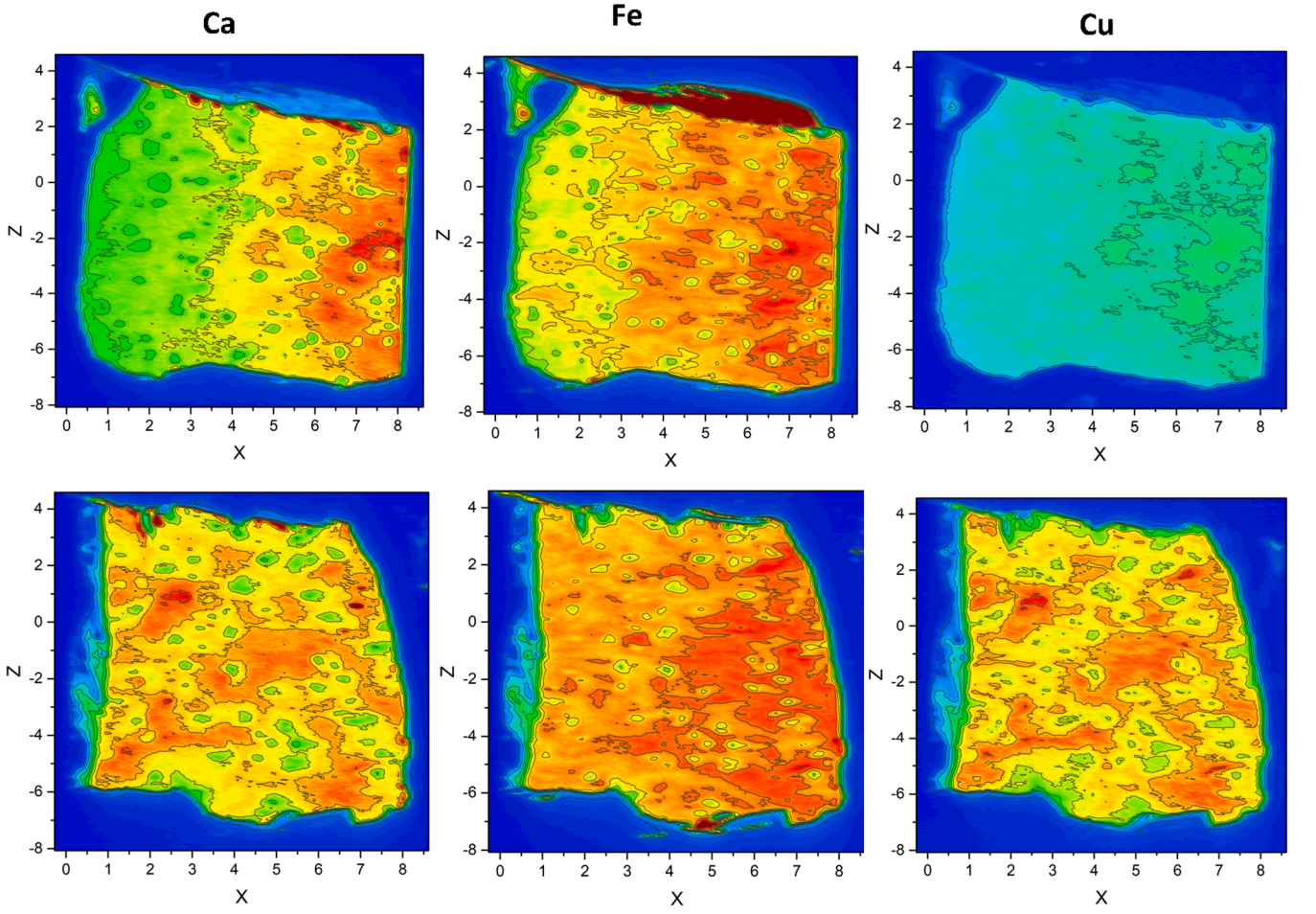

Fig. 3. X-Ray Fluorescence maps corresponding to calcium, iron and copper for JS24 (Top) blue glaze and (Bottom) red glaze. The intensities are the same for each element. (For interpretation of the references to colour in this figure legend, the reader is referred to the web version of this article.)

Electron Images (SE) were obtained, acceleration voltage 5 kV. The chemical composition was measured by Energy Dispersive X-Ray Spectroscopy detector (EDS) (INCAPentaFETx3, 30 mm^2, ATW2 window and mineral and glass standards) attached to the SEM, acceleration voltage 20 kV, with 120 s measuring times.

Ultra-Violet and Visible (UV-Vis) diffuse reflectance measurements were obtained from the surface of the glazes using a double beam spectrophotometer (Shimadzu 2700) equipped with ISR 3100 Ulbricht integrating sphere (spot size of 3 mm x 1 mm and 1 nm resolution, D65 standard illumination source, barium sulphate provided a white standard).

3. Results and discussion

The Fe K-edge pre-edge peaks of the XAS data gives information on the oxidation state and coordination of iron. First of all, a collection of standards was measured and fitted to validate the fitting procedure used. The corresponding fitted data is shown in the supplementary materials, Table S1 and Fig. S1 and the variogram in supplementary materials Fig. S2. The values obtained are in good agreement with those obtained by other authors [22,27].

The Fe K-edge pre-edge fitted peaks from the blue glazes (JS24, JS26, JS27, JS77 and JS4) and the brown glaze (JS78) are shown in Fig. 2 and Fig. S3 respectively and the corresponding parameters, Fe^{3+} and Fe^{2+} peak positions and areas (E_1, E_2, A_1 and A_2), the centroid (C) and total area (A) and relative data of the Fe^{2+} peak (A(Fe^{2+}/Fe)) obtained are

Table 2
Fitted pre-edge peaks corresponding to the blue (B) and red (R) glazes in calcium rich (R) and poor (P) areas.

JS24			fwhm		Fe^{3+}			Fe^{2+}			C		A		$A\ (Fe^{2+}/Fe)^a$		Fe^{2+}/Fe_{total} [1]	
			(eV)		E_1 (eV)		A_1 (eV)		E_2 (eV)	A_2 (eV)	(eV)		(eV)				(%)	
Blue	Ca-rich	BR1	1.79	(2)	7114.44	(1)	0.200	(3)	7112.45	(8)	0.028	(2)	7114.20	(1)	0.228	(3)	0.121	(2)	20	(3)
		BR2	1.77	(2)	7114.44	(1)	0.198	(2)	7112.44	(8)	0.026	(1)	7114.21	(1)	0.224	(3)	0.115	(1)	17	(3)
	Ca-poor	BP1	1.71	(3)	7114.43	(1)	0.158	(3)	7112.54	(6)	0.041	(2)	7114.04	(2)	0.199	(4)	0.206	(2)	70	(5)
		BP2	1.77	(3)	7114.43	(2)	0.167	(3)	7112.46	(7)	0.038	(2)	7114.07	(2)	0.205	(4)	0.185	(2)	57	(5)
Red	Ca-rich	RR1	1.79	(2)	7114.44	(1)	0.200	(2)	7112.45	(7)	0.024	(1)	7114.23	(1)	0.224	(3)	0.106	(1)	11	(3)
		RR2	1.78	(1)	7114.46	(1)	0.202	(2)	7112.40	(7)	0.023	(1)	7114.25	(1)	0.225	(2)	0.100	(1)	8	(3)
	Ca-poor	RP1	1.76	(2)	7114.45	(1)	0.195	(3)	7112.45	(6)	0.029	(1)	7114.19	(1)	0.224	(2)	0.128	(1)	24	(3)
		RP2	1.77	(2)	7114.45	(1)	0.179	(3)	7112.50	(7)	0.036	(2)	7114.12	(2)	0.215	(4)	0.167	(2)	47	(4)

shown in Table 1 and the variogram in supplementary materials Fig. S2. Mössbauer data obtained from the blue glazes JS77 and JS4 and the brown glaze JS78 [4] were used to calibrate the Fe^{2+} content and are also shown in Table 1.

The data corresponding to the blue glazes show a relatively good correlation with the average calcium content of the glazes as is shown in Fig. 2. The calcium rich glazes appear more oxidized than the calcium poorer glazes (supplementary materials Fig. S4).

However, the heterogeneous submillimetric lime rich and poor structures shown by the glazes are large enough to affect the data obtained. For this reason, a smaller beam size was selected and an X-ray Fluorescence map was obtained from the blue glaze of JS24. Fig. 3 shows the corresponding fluorescence maps of Fe and Ca which show a good correlation. Generally speaking, the calcium rich areas are also iron rich while calcium poor areas are iron poor. In fact, in a previous study, lime rich droplets were found to be also iron rich while the silica rich (and lime poor) were also iron poor [4]. Therefore, the X-ray Fluorescence data showing that iron is concentrated in the calcium rich areas of the glaze confirms that the lime rich droplets are also iron richer.

Moreover, the pre-edge fitted data is shown in Table 2 and the spectra corresponding to a calcium rich and a calcium poor area in Fig. 4. The data shows that iron appears also more oxidized in the calcium rich areas suggesting that lime rich droplets incorporate more Fe^{3+} than the silica rich droplets.

Fig. 1 shows a SEM image of the glass nanostructure developed in the blue glaze from JS24. Calcium richer areas have more and larger droplets than calcium poorer areas. This side of JS24 contains some copper but below 0.1% CuO even in the richest areas. Previous analyses of the droplets and the matrix of the glaze [4] have shown that the glass droplets are enriched in Ca, Mg, Fe, P and Ti (about 3 times those of the matrix) while the matrix is enriched in Si, Na and K. A simultaneous oxidation of Fe^{2+} into Fe^{3+} and reduction of Ti^{4+} into Ti^{3+} which has been observed at the glaze in contact with the ceramic, suggests that the higher concentration of titanium in the calcium rich droplets may also be responsible of the greater oxidation of iron in the calcium rich areas.

Both calcium rich and poor areas of the red glaze were also measured and the fitted parameters and spectra are also shown in Table 2 and Fig. 4 respectively. The copper content in this side is 0.2%CuO, which is associated with the presence of 0.3%SnO_2 and 0.2% PbO which indicates the reuse of bronze. We can see that the iron in the calcium rich and poor areas of the red glaze is more oxidized (10–12% Fe^{2+} and 24–47% Fe^{2+}) than the corresponding calcium rich and poor areas of the blue glaze (17–20% Fe^{2+} and 57–70% Fe^{2+}). Fig. 1 shows the nanostructure developed in the calcium-rich areas of the JS24 red glaze. Although the nanostructure is the same, a few copper nanoparticles, absent in the blue area, are found in the red area. The copper particles are formed at the interface between the droplets and the matrix.

UV-Vis data was also obtained from the blue and the red sides of JS24. Besides the small copper content present in the red side (0.2% CuO) and the scarcity and small size of the copper nanoparticles, the Surface Plasmon Resonance (SPR) absorption is an important contribution to the scattering contribution of the glass nanostructure and Fe^{2+} absorption characteristic of the blue glaze (Fig. 5).

The position of the absorption XANES edge shifts characteristically with oxidation state (8982.3 eV for Cu°, 8983.8 eV for cuprite, Cu^{+} and 8986.9 eV for tenorite, Cu^{2+}). From the XANES spectrum (Fig. 6) it is quite evident that Cu is present mainly as Cu^{+} due to the absence of a 1s→3d transition and the intense feature at 8983 eV.

The copper K-edge and the 1st derivative XANES spectra from copper standards and the blue and red areas of JS24 are shown in Fig. 6. Copper K-edge XANES spectra of both Cu^{2+} and Cu^{+} contain features characteristic of the oxidation state and speciation [30]. The pre-edge feature which corresponds to dipole-forbidden electronic transitions from core 1 s levels to the first empty 3d states (but hybridized by 2p orbitals of the O ligands). For Cu^{0} and Cu^{+} in Cu_2O, there is no empty 3d initial states, so the pre-edge is the signature of Cu^{2+}. Due to only one empty 3d

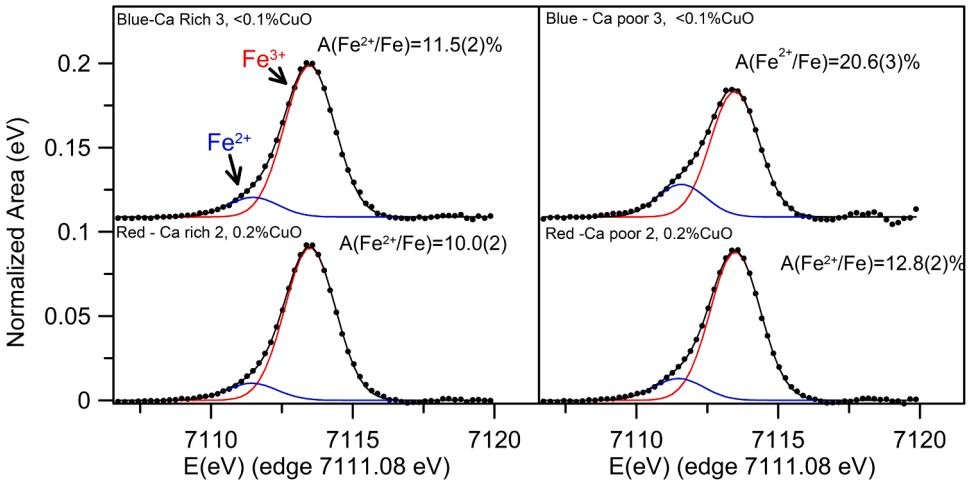

Fig. 4. Fitted pre-edge peaks corresponding to the calcium rich and poor areas of the blue and red JS24 glazes.

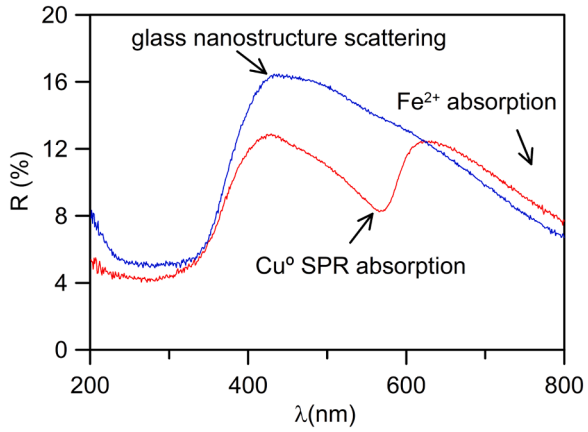

Fig. 5. UV-Vis spectra from the Blue and Red sides of JS24. The large scattering contribution between 400 nm and 600 nm from the droplets structure and the broad absorption of Fe^{2+} (maximum at ≈1100 nm) extending to the red part of the visible spectra is also clearly seen. In the red side the Surface Plasmon Resonance Absorption peak corresponding to metal copper nanoparticles ($\lambda_p \approx$ 560 nm) is clearly seen. (For interpretation of the references to colour in this figure legend, the reader is referred to the web version of this article.)

orbital to accept the excited 1s electron, the feature has an extremely weak intensity.

Fig. 6 shows no pre-edge features characteristic of metallic copper (Cu^0), Cu^+ in cuprite or Cu^{2+} in tenorite. The feature located near 8982 eV is attributed to the 1s→4p electric dipole transition and is often considered a signature of Cu^+ [31]. Actually, this transition is intense and sharp in cuprite (Cu_2O), in which the copper atoms are located in a linear geometry (2-coordinated by oxygens) [32]. The edge shift between Cu^+ and Cu^{2+} is typically large (>5 eV) and derives from an intense Cu^+ pre-edge feature (1s → 4p) that merges with, and is usually referred to as, the absorption edge [33]. Features comprising the edge are often more easily identified in the derivative spectra, shown also in Fig. 6, in which inflections appear as peaks. The energy positions of the feature discriminate between Cu^+ and Cu^{2+}. In general, Fig. 6 shows the expected shift of absorption edge to higher energy with increasing oxidation state and differences in the edge shape.

EXAFS data was fitted to determine the distances, coordination number, and neighbour atoms. The signal corresponding to the Cu-Cu bond length could not be fitted, probably because of the few particles present, their small size and their large surface/volume ratio. The copper atoms at the particles surface have other atoms than copper as near neighbours, this reduces even further their contribution to the EXAFS spectra. The k^3 weight k-space and R-space experiment data (points) and the corresponding fits (solid lines) of a calcium poor area from the blue glaze (BP2) are shown in Fig. 7. Full results of the fitting of the spectra are given in Table 3 together with the crystallographic information corresponding to cuprite (ID: mp-361; DOI: 10.17188/1207131) and tenorite (code COD: 9014580). The R factor gives the misfit and it is used as an estimator for the goodness of the fitting.

The data indicates that copper is mainly present as Cu^+ and Cu^{2+} appearing more oxidised in the calcium rich areas, $Cu^+/(Cu^+ + Cu^{2+}) \approx 0.6–0.7$, than in the calcium poor areas, $Cu^+/(Cu^+ + Cu^{2+}) \approx 0.8–0.9$. The ratio in the red and the blue glazes is essentially the same. We know that in the red side we also have copper nanoparticles. However, the copper nanoparticles are so few and their size so small that it has been not possible to identify the corresponding back-scattering paths in the EXAFS signal.

Copper is dissolved in a glaze as Cu^+ and Cu^{2+}, the relative ratio of both depends on the composition of the glass and on the firing atmosphere. The composition of both, the blue and the red side is equivalent in the calcium rich and calcium poor areas and the firing atmosphere was the same. Consequently, the reduction of copper to the metallic state and precipitation of copper metal nanoparticles can only be related to simultaneous oxidation of the other transition metal ions present, iron and titanium. The reduction of copper from Cu^+ to Cu^o is obtained by the simultaneous oxidation of Fe^{2+} to Fe^{3+}. In fact, iron appears more oxidised in the red glaze (24–47% Fe^{2+} in the calcium rich areas and 8–11% Fe^{2+} in the calcium poor areas) than in the blue side (57–70% Fe^{2+} in the calcium rich areas and 17–20% Fe^{2+} in the calcium poor areas).

The *sky*-like appearance shown by the blue Jun ware glazes is due to the combination of transparent-blue and whitish-opaque submillimetre areas: the presence of large droplets in the calcium rich areas increases the light scattered, resulting in an opaque glaze, while in the calcium poor areas containing small droplets the light is mainly absorbed in the silica-matrix, resulting in a transparent glaze. Now we have demonstrated that iron is more reduced in the calcium poor transparent areas than in the calcium rich opaque areas (57–70% Fe^{2+} instead of 17–20% Fe^{2+}). This indicates also that iron is more oxidised in the lime-rich droplets than in the silica-rich matrix where it appears mainly as Fe^{2+}. The concentration of titanium in the calcium rich droplets explains why iron is more oxidised. Moreover, the reduced content of titanium in the silica matrix explains why, even in Jun glazes with TiO_2 above 0.2%, the transparent areas of the glazes appear blue instead of green.

Consequently, the calcium rich areas where the iron is mainly oxidised will appear white-cream opaque, and the calcium poor areas

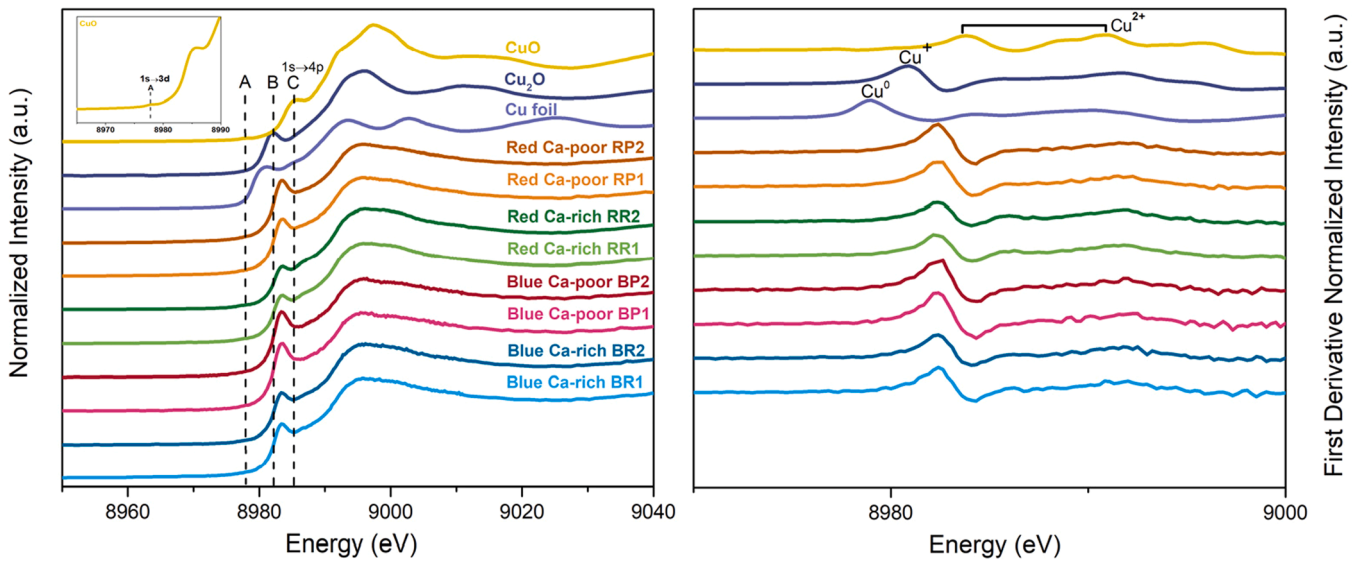

Fig. 6. (left) Cu K-edge XANES spectra and (right) 1st derivative XANES spectra from the blue and red areas of JS24. (For interpretation of the references to colour in this figure legend, the reader is referred to the web version of this article.)

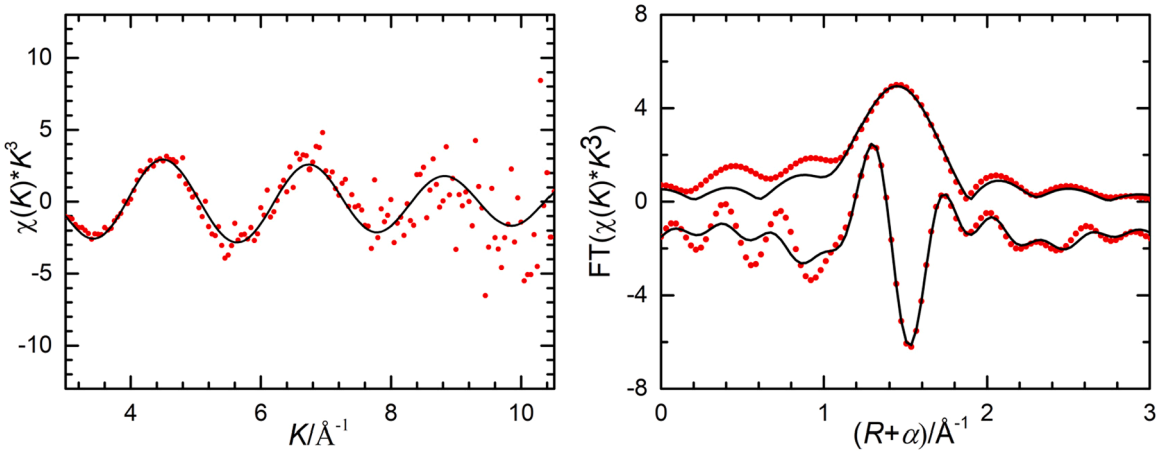

Fig. 7. Cu K-edge experimental data (points) and curvefit (line) of BP2 (left) k^3-weighted phase-uncorrected data. (right) R-space (FT magnitude and Imaginary component).

Table 3
Curvefit parameters[a] for Cu K-edge EXAFS for JS24 glazes.

JS24			Path	N[b]	R/ Å	$\sigma^{2\,(c)}$/ Å^2	R[d] factor (%)	$Cu^+/(Cu^+ + Cu^{2+})$
Blue	Ca-rich	BR1	Cu-O1	2.0	1.84(1)	0.003(2)	0.6%	0.7(1)
			Cu-O2	4.0	1.94(1)	0.003(2)		
		BR2	Cu-O1	2.0	1.84(2)	0.003(3)	2.1%	0.7(2)
			Cu-O2	4.0	1.94(2)	0.003(3)		
	Ca-poor	BP1	Cu-O1	2.0	1.87(1)	0.002(1)	0.2%	0.89(6)
			Cu-O2	4.0	1.97(1)	0.002(1)		
		BP2	Cu-O1	2.0	1.86(1)	0.002(1)	0.5%	0.87(9)
			Cu-O2	4.0	1.96(1)	0.002(1)		
Red	Ca-rich	RR1	Cu-O1	2.0	1.84(1)	0.003(1)	0.2%	0.65(8)
			Cu-O2	4.0	1.94(1)	0.003(1)		
		RR2	Cu-O1	2.0	1.83(1)	0.004(1)	0.3%	0.6(1)
			Cu-O2	4.0	1.93(1)	0.004(1)		
	Ca-poor	RP1	Cu-O1	2.0	1.85(1)	0.003(1)	0.9%	0.8(1)
			Cu-O2	4.0	1.95(1)	0.003(1)		
		RP2	Cu-O1	2.0	1.86(1)	0.003(1)	0.2%	0.84(7)
			Cu-O2	4.0	1.96(1)	0.003(1)		

[a] S_o^2 was obtained from the analysis of Cu foil and fixed to 0.81. Data ranges: 3.0 ≦k ≦ 10.5 Å^{-1}, 1.0 ≦R≦ 2.3 Å. [b] These coordination numbers were constrained as N (Cu-O1)= 2 and N(Cu-O2)= 4 based on the crystal structure of Cu_2O and CuO. [c] The Debye-Waller factors were constrained as σ^2(Cu-O1)= σ^2(Cu-O2) to decrease variable parameters. [d] R factor is the goodness of fit parameter.

where the iron is mainly reduced will appear transparent blue. Finally, the combination of both effects is a blue glaze with white opaque areas, a sky with clouds appearance.

The high absorbance associated to the Surface Plasmon Resonance at $\lambda \approx 560$ nm of copper metal nanoparticles is responsible for the red and violet colour to the white/yellowish and blue areas of the glaze respectively even if very few nanoparticles are present.

4. Conclusions

A glass nanostructure is developed in Jun ware glazes due to the high SiO_2:Al_2O_3 ratio (above 7:1), which, when fired at temperatures of about 1200 °C, undergoes a liquid-liquid phase separation. A double glass nanostructure, lime-rich (enriched also in Fe, Mg, P and Ti) droplets in a silica-rich matrix (enriched also in K and Na) is developed. A XAS study has demonstrated that iron is more oxidised in the calcium rich areas than in the calcium poor areas of the glaze, $\approx$ 17–20% Fe^{2+} and $\approx$ 60–70% Fe^{2+} respectively, implying that iron is predominantly oxidised in the lime-rich droplets and reduced in the silica-rich matrix.

Consequently, the *sky*-like appearance shown by the blue Jun ware glazes is due to the combination of the light absorption in the transparent-dark-blue Fe^{2+} rich and titanium poor areas and light scattering in the white-yellowish Fe^{3+} rich areas.

Copper was also added to the glazes to imprint red/violet colours. Copper appears mainly as Cu^{+} and Cu^{2+} in the glaze, the ratio between both is known to depend on the composition of the glaze and atmosphere. Iron is more oxidised in the red glaze where copper metal nanoparticles are present than in the blue glaze where they are absent. This effect is more pronounced in the calcium poor areas (containing more Fe^{2+}) than in the calcium rich areas (containing more Fe^{3+}). The results obtained point out to the simultaneous reduction of copper from Cu^{+} to Cu^{o} and oxidation of iron from Fe^{2+} to Fe^{3+}.

Declaration of Competing Interest

The authors declare that they have no known competing financial interests or personal relationships that could have appeared to influence the work reported in this paper.

Acknowledgments

The project received financial support from MINECO (Spain) (grant PID2019–105823RB-I00) and Generalitat de Catalunya (grant 2017 SGR 0042). The experiments were performed at BL22 (CLAESS) Beamline at ALBA synchrotron Facility with the collaboration of Alba Staff, project number 2019093906.

Appendix A. Supporting information

Supplementary data associated with this article can be found in the online version at doi:10.1016/j.jeurceramsoc.2022.02.016.

References

[1] R. Tichane, Those Celadon Blues, Institute for Glaze Research, New York State, US, 1978.
[2] N. Wood, Chinese Glazes: Their Origins. Chemistry and Recreation, A&C Black, London, UK, 1999.
[3] N. Wood, Some Mysteries of Jun Ware Manufacture, Junyao, Eskenazi, London, UK, 17–28, 2013.
[4] J.Y. Hou, T. Pradell, Y. Li, J.M. Miao, Jun ware glazes: chemistry, nanostructure and optical properties, J. Eur. Ceram. Soc. 38 (2018) 4290–4302, https://doi.org/10.1016/j.jeurceramsoc.2018.05.010.
[5] W.D. Kingery, P.B. Vandiver, Song Dynasty Jun (Chün) ware glazes, Am. Ceram. Soc. Bull. 62 (11) (1983) 1269–1274.
[6] W.D. Kingery, P.B. Vandiver, I.W. Huang, Y.M. Chiang, Liquid-liquid immiscibility and phase separation in the quaternary systems K_2O-Al_2O_3-CaO-SiO_2 and Na_2O-Al_2O_3-CaO-SiO_2, J. Non-Cryst. Solids 54 (1983) 163–171, https://doi.org/10.1016/0022-3093(83)90090-X.
[7] X.Q. Chen, R.F. Huang, S.P. Chen, X. Zhou, Chinese Phase Separated Glazes in Successive Dynasties-their Chemical Composition, Immiscible Structure and Artistic Appearance, In: J. Li & X. Chen (Eds.), Proceedings of the 1989 International Symposium on Ancient Ceramics Shanghai, China (1989) 31–37.
[8] P.B. Vandiver, Variability of Song Dynasty Green Glaze Technology Using Microstructure, Microcomposition and Thermal History to Compare Yaozhou, Jun, Ru, Yue, Longquan, Guan, and Korean Koryo Dynasty Materials and Practices, The Palace Museum. Beijing, China, Proceedings of International Symposium on Science and Technology of Five Great Wares of the Song Dynasty (2016) 391–432.
[9] Y.M. Chiang, W.D. Kingery, Spinodal decomposition in a K_20-Al_20_3-Ca0-$Si0_2$, Glass, Commun. Am. Ceram. Soc. 66 (9) (1983) c171–c172, https://doi.org/10.1111/j.1151-2916.1983.tb10632.x.
[10] E. Roedder, Liquid immiscibility in K_2O-FeO-Al_2O_3–SiO_2, Nature 267 (1977) 558–559, https://doi.org/10.1038/267558b0.
[11] E. Roedder, Fluid inclusion evidence for immiscibility in magmatic differentiation, Geochim. Cosmochim. Acta 56 (1992) 5–20, https://doi.org/10.1016/0016-7037(92)90113-W.
[12] A.R. Philpotts, Compositions of immiscible liquids in volcanic rocks, Contrib. Mineral. Petrol. 80 (1982) 201–218, https://doi.org/10.1007/BF00371350.
[13] W.A. Weyl, Coloured Glasses. Sheffield: Society of Glass Technology, UK, 1951.
[14] D. Ehrt, M. Leister, A. Matthai, Polyvalent elements iron, tin and titanium in silicate, phosphate and fluoride glasses and melts, Phys. Chem. Glass 42 (3) (2001) 231–239.
[15] J.Y. Kim, H.G. No, A.Y. Jeon, U.S. Kim, J.H. Pee, W.S. Cho, K.J. Kim, C.M. Kim, C. S. Kim, Mössbauer spectroscopic and chromaticity analysis on colorative mechanism of celadon glaze, Ceram. Int. 37 (2001) 3389–3395, https://doi.org/10.1016/j.ceramint.2011.05.141.
[16] A.Y. Jeon, H.G. No, U.S. Kim, W.S. Cho, G.I. Kang, Mössbauer spectroscopic and chromaticity analysis on the colourative mechanism of ancient goryeo celadon from gangjin and buan, Archaeometry 56 (3) (2014) 392–405, https://doi.org/10.1111/arcm.12032.
[17] N. Wood, Nought-point-two per cent titanium dioxide: a key to song ceramics? J. Archaeol. Sci. Rep. 35 (2021), 102727 https://doi.org/10.1016/j.jasrep.2020.102727.
[18] U. Kreibig, M. Vollmer, Optical properties of metal cluster. Springer series 25, Springer, Berlin, Germany, 1995.
[19] Q.Y. Zhao, The excavation of Juntai Kiln, Yuzhou, Henan Province, J. Cult. Relics (文物) 6 (1975) 57–64, https://doi.org/10.13619/j.cnki.cn11-1532/k.1975.06.006.
[20] L. Simonelli, C. Marini, W. Olszewski, M. Ávila Pérez, N. Ramanan, G. Guilera, V. Cuartero, K. Klementiev, CLÆSS: The hard X-ray absorption beamline of the ALBA CELLS synchrotron, Cogent Phys. 3 (2016), 1231987, https://doi.org/10.1080/23311940.2016.1231987.
[21] B. Ravel, M. Newville, ATHENA, ARTEMIS, HEPHAESTUS: Data Analysis for X-Ray Absorption Spectroscopy Using IFEFFIT, J. Synchrotron Radiat. 12 (4) (2005) 537–541, https://doi.org/10.1107/S0909049505012719.
[22] M. Wilke, F. Farges, P. Petit, G.E.Jr Brown, F. Martin, Oxidation state and coordination of Fe in minerals: An Fe K-XANES spectroscopic study, Am. Mineral. 86 (5) (2001) 714–730, https://doi.org/10.2138/am-2001-5-612.
[23] M. Wilke, G.M. Partzsch, R. Bernhardt, D. Lattard, Determination of the iron oxidation state in basaltic glasses using XANES at the K-edge, Chem. Geol. 220 (2005) 143–161, https://doi.org/10.1016/j.chemgeo.2005.03.004.
[24] F. Farges, Y. Lefrère, S. Rossano, A. Berthereau, G. Calas, G.E. Brown Jr, The effect of redox state on the local structural environment of iron in silicate glasses: a combined XAFS spectroscopy, molecular dynamics, and bond valence study, J. Non-Cryst. Solids 344 (3) (2004) 176–188, https://doi.org/10.1016/j.jnoncrysol.2004.07.050.
[25] J.L. Knipping, H. Behrens, M. Wilke, J. Goettlicher, P. Stabile, Effect of oxygen fugacity on the coordination and oxidation state of iron in alkali bearing silicate melts, Chem. Geol. 411C (2015) 143–154, https://doi.org/10.1016/j.chemgeo.2015.07.004.
[26] O.L.G. Alderman, L. Lazareva, M.C. Wilding, C.J. Benmore, S.M. Heald, C. E. Johnson, J.A. Johnson, H.Y. Hah, S. Sendelbach, A. Tamalonis, L.B. Skinner, J. B. Parise, J. Weber, Local structural variation with oxygen fugacity in Fe_2SiO_{4+x} fayalitic iron silicate melts, Geochim. Cosmochim. Acta 203 (2017) 15–36, https://doi.org/10.1016/j.gca.2016.12.038.
[27] A. Boubnov, H. Lichtenberg, S. Mangold, J.D. Grunwaldt, Identification of the iron oxidation state and coordination geometry in iron oxide- and zeolite-based catalysts using pre-edge XAS analisis, J. Synchrontron Radiat. 22 (2015) 410–426, https://doi.org/10.1107/S1600577514025880.
[28] E. Jones, T. Oliphant, P. Peterson and others, SciPy: Open Source Scientific Tools for Python. Curve_fit, 2001. ⟨https://docs.scipy.org/doc/scipy/reference/generated/scipy.optimize.curve_fit.html⟩.
[29] S. Calvin. XAFS for Everyone, 1st ed..,, CRC Press, 2013, pp. 342–343.
[30] A.J. Berry, A.C. Hack, J.A. Mavrogenes, M. Newville, S.R. Sutton, A XANES study of Cu speciation in high-temperature brines using synthetic fluid inclusions, Am. Mineral. 91 (2006) 1773–1782, https://doi.org/10.2138/am.2006.1940.
[31] C. Maurizio, F. d'Acapito, M. Benfatto, S. Mobilio, E. Cattaruzza, F. Gonella, Local coordination geometry around Cu and Cu ions in silicate glasses: an X-ray absorption near edge structure investigation, Eur. Phys. J. B 14 (2000) 211–216, https://doi.org/10.1007/s100510050122.
[32] R. Restori, D. Schwarzenbach, Charge density in cuprite, Cu_2O, Acta Cryst. B42 (1986) 201–208, https://doi.org/10.1107/S0108768186098336.
[33] J.L. Fulton, M.M. Hoffmann, J.G. Darab, An X-ray absorption fine structure study of copper(I) chloride coordination structure in water up to 325°C, Chem. Phys. Lett. 330 (2000) 300–308, https://doi.org/10.1016/S0009-2614(00)01110-6.